Membrane-Based Ethylene/Ethane Separation: The Upper Bound and Beyond

Meha Rungta, Chen Zhang, and William J. Koros
School of Chemical and Biomolecular Engineering, Georgia Institute of Technology, Atlanta, GA 30332

Liren Xu
The Dow Chemical Co., Freeport, TX 77541

DOI 10.1002/aic.14105
Published online August 2, 2013 in Wiley Online Library (wileyonlinelibrary.com)

Ethylene/ethane separation via cryogenic distillation is extremely energy-intensive, and membrane separation may provide an attractive alternative. In this paper, ethylene/ethane separation performance using polymeric membranes is summarized, and an experimental ethylene/ethane polymeric upper bound based on literature data is presented. A theoretical prediction of the ethylene/ethane upper bound is also presented, and shows good agreement with the experimental upper bound. Further, two ways to overcome the ethylene/ethane upper bound, based on increasing the sorption or diffusion selectivity, is also discussed, and a review on advanced membrane types such as facilitated transport membranes, zeolite and metal organic framework based membranes, and carbon molecular sieve membranes is presented. Of these, carbon membranes have shown the potential to surpass the polymeric ethylene/ethane upper bound performance. Furthermore, a convenient, potentially scalable method for tailoring the performance of carbon membranes for ethylene/ethane separation based on tuning the pyrolysis conditions has also been demonstrated. © 2013 American Institute of Chemical Engineers *AIChE J*, 59: 3475-3489, 2013

Keywords: ethylene/ethane, polymeric upper bound, facilitated transport, zeolite, metal organic framework, carbon molecular sieve, pyrolysis

Introduction

Ethylene/ethane (C_2H_4/C_2H_6) separations are currently carried out using energy intensive distillation operations,[1,2] and have long been identified as applications where low-energy separation replacements could provide very large (on the order of 10^{12} Btu/y) reductions in energy consumption.[1,3–5] Alternative less energy-intensive separation technologies, such as membranes, adsorption, absorption and extraction, have been important areas of research, and the concept of hybrid systems has drawn significant attention. Several limitations, however, have prevented the adoption of these technologies to replace or complement cryogenic distillation processes.[2] The greatest limitations to the application of membrane separation technology for distillation are their lack of selectivity, their narrow range of useful operation conditions and their high costs.[2,6–8] Currently explored membrane materials for C_2H_4/C_2H_6 separation lack either the separation performance or the stability required to successfully implement hybrid membrane-distillation concepts.[5] Conventional polymeric membranes cannot achieve the productivity (permeability) and efficiency (selectivity) combinations required for C_2H_4/C_2H_6 separations.[9–12] In this regard, understanding the tradeoff between C_2H_4/C_2H_6 selectivity vs. C_2H_4 permeability for polymeric membrane materials, and the limit to this tradeoff defined by hyper-rigid glassy polymers, can allow exploring options for new high-performing membrane materials for C_2H_4/C_2H_6 separations. In addition, for most polymeric materials, the membrane stability under actual aggressive hydrocarbon feeds requires consideration. Because of these concerns, olefin/paraffin separation applications might be one for which the benefits of inorganic membranes may justify their higher costs.[6,13] These concerns and opportunities stimulated our work on carbon molecular sieve (CMS) membrane materials for C_2H_4/C_2H_6 separation, which is discussed.

Theory and Background

Gas transport in polymeric membranes follows a sorption-diffusion model, wherein the gas molecules sorb onto the upstream of the membrane, diffuse through the membrane under a chemical potential gradient, and desorb at the downstream. The permeability (productivity) of a membrane is defined as the pressure and thickness normalized flux

$$P_A = \frac{N_A \, \ell}{\Delta p_A} \tag{1}$$

Permeability is typically given in the units of Barrer, where

$$1 \quad \text{Barrer} = 10^{-10} \frac{\text{cc (STP)}.\text{cm}}{\text{cm}^2.\text{s.cmHg}} \tag{2}$$

Correspondence concerning this article should be addressed to W. J. Koros at wjk@chbe.gatech.edu.

Another popular unit for permeability is $\frac{\text{kmol .m}}{\text{m}^2.\ \text{s}\ .\text{kPa}}$ $\left(1\ \text{Barrer} = 3.44\times10^{-16}\frac{\text{kmol .m}}{\text{m}^2.\ \text{s}\ .\text{kPa}}\right)$.

Permeability can further be represented as the product of a thermodynamic sorption coefficient ($\bar{S}_A$), and a kinetic diffusion coefficient ($\bar{D}_A$).

$$P_A = \bar{D}_A \bar{S}_A \tag{3}$$

The permselectivity (or ideal selectivity) of the membrane is the ratio of the pure gas permeabilities of the fast gas (A) over the slow gas (B), for the case where the downstream pressure is negligible relative to the upstream feed pressure. The permeability can also be represented as the product of the sorption and diffusion selectivities.

$$\alpha_{A/B} = \frac{P_A}{P_B} = \left(\frac{\bar{D}_A}{\bar{D}_B}\right)\left(\frac{\bar{S}_A}{\bar{S}_B}\right) \tag{4}$$

The membrane literature has identified a tradeoff line between permeability and selectivity for separation of gases using easily processed polymeric membranes. This tradeoff relationship shows that the separation factor for a gas pair (A/B) of interest varies inversely with the permeability of the faster gas (A). This is referred to as an "upper bound" [14–16] and is typically represented on a log–log plot of α vs. P.

$$\alpha_{A/B} = \frac{\beta_{A/B}}{P_A^{\lambda_{A/B}}} \tag{5}$$

In 1991, Robeson[14] defined the upper bound for several gas pairs from the list of He, H_2, O_2, N_2, CO_2 and CH_4 based on a thorough analysis of literature data. He identified a linear relationship between the slope of the upper bound and the difference of the Lennard-Jones kinetic diameters of the given gas pair, thus, indicating the dominance of a diffusion-based separation of these gas pairs for high-performing polymers that define the upper bound. Continuous efforts to improve gas transport properties of hyper-rigid glassy polymers by tailoring their structure, and fluorinated polymers have successfully shifted the upper bound.[15]

In 1999, Freeman[16] presented a fundamental analysis of the upper bound line for polymeric membrane materials, and presented a way to predict the slope ($\lambda_{A/B}$) and front factor ($\beta_{A/B}$) of the upper bound line as follows

$$\lambda_{A/B} = \left(\frac{d_B}{d_A}\right)^2 - 1 \tag{6}$$

and

$$\beta_{A/B} = \frac{S_A}{S_B} S_A^{\lambda_{A/B}} \exp\left\{-\lambda_{A/B}\left[b - f\left(\frac{1-a}{RT}\right)\right]\right\} \tag{7}$$

In Eq. 6, d_A and d_B represent the kinetic diameters of the fast gas (A) and slow gas (B), respectively. As observed by Robeson,[14,15] Eq. 6 directly suggests that the slope of the upper bound is a natural consequence of the size-sieving nature of stiff chain glassy polymers that generally define the upper bound. In Eq. 7, S_A and S_B represent the sorption coefficients of the gases; the parameter f relates to interchain spacing and its value ranges from 0 for rubbery and low-performance glassy polymers to $\approx$14,000 cal/mol (1 cal/mol = 4.184 J/mol) for high-performance rigid polyimides[16,17]; a and b are linear free energy coefficients that correlate the diffusion front factor (D_{oA}) to the activation energy of diffusion (E_{oA}) as follows[18,19]

Table 1. C_2H_4/C_2H_6 Separation Performance for Polymeric Membranes[a]1 atm = 101.325 kPa

Precursor	T	p	P_{C2H4}	$\alpha_{C2H4/C2H6}$	Source
	°C	atm[a]	Barrer		
6FDA-6FpDA	35	5.0	1.90	4.20	9
6FDA-1,5-NDA	35	5.0	0.87	5.80	
6FDA-NDA	35	2.0	1.17	6.84	10
6FDA-NDA/Durene (75:25)	35	2.0	4.46	5.62	
6FDA-NDA/Durene (50:50)	35	2.0	9.48	4.27	
6FDA-NDA/Durene (25:75)	35	2.0	36.70	3.60	
6FDA-Durene	35	2.0	76.70	2.89	
6FDA-TrMPD	50	2.0	58.00	2.90	11
BPDA-TeMPD	50	2.0	5.80	4.30	
6FDA-mPD	35	3.8	0.30	3.30	12
6FDA-IPDA	35	3.8	1.40	3.80	
6FDA-6FpDA	35	3.8	2.10	4.40	
Matrimid®	35	3.4	0.45	4.50	This
6FDA-DAM	35	3.4	64.00	3.00	work
6FDA:BPDA-DAM	35	3.4	46.00	3.30	

[a]1 atm = 101.325 kPa

$$\ln D_{oA} = a\frac{E_{DA}}{RT} - b \tag{8}$$

a and b are independent of gas type, with a being independent of polymer type as well and having a universal value of 0.64[20]; b has a value of $-\ln(10^{-4}$ cm^2/s) (1 cm^2/s = 10^{-4} m^2/s) for rubbery polymers and $-\ln(10^{-5}$ cm^2/s) for glassy polymers.[21] In the above equations, R represents the universal gas constant, and T represents the absolute temperature.

The equations above allow predicting the slope (λ) of the upper bound with no adjustable parameters and the front factor (β) with only one adjustable parameter. As shown by Freeman,[16] predictions of λ and β from the aforementioned equations furnished a good correlation with the slopes and front factors presented by Robeson[14,15] for several gas pairs.

In 2003, Burns and Koros[22] presented the upper bound for C_3H_6/C_3H_8 separations. In this article, we present an experimental C_2H_4/C_2H_6 upper bound based on literature data, as well as extend the analysis by Freeman[16] to predict the C_2H_4/C_2H_6 upper bound for polymeric membrane materials. Further we also consider approaches to overcome the upper bound line and advanced membrane types for C_2H_4/C_2H_6 separation.

Experimental C_2H_4/C_2H_6 Upper Bound

Limited work has been done in the field of polymeric membrane-based C_2H_4/C_2H_6 separations and, as such, a comprehensive summary focusing solely on C_2H_4/C_2H_6 separation has not been presented or reviewed. Recently we published a compilation of literature data available for C_2H_4/C_2H_6 separation using polymeric membranes,[5,9–12,23] as well as included measurements on polymers used in this work. This data is shown in Table 1. Table 2 lists the chemical names for abbreviations used for polymers in Table 1.

Based on the data shown in Table 1 we plotted an experimental C_2H_4/C_2H_6 tradeoff line, shown in Figure 1.

All measurements reported in Table 1 are based on pure gas steady-state permeation tests using dense films between 35 and 50°C and 2–5 atm (1 atm = 101.325 kPa) feed

Table 2. Chemical Names for Abbreviations in Table 1

Abbreviation	Chemical Name
6FDA	4,4'-(hexafluoroisopropylidene) dipthalic anhydride
6FpDA	4,4'-(hexafluoroisopropylidene) dianiline
NDA	1,5-naphthalene diamine
Durene	1,2,4,5-tetramethylbenzene
TrMPD (DAM)	2,4,6-trimethyl-1,3-phenylene diamine
BPDA	3,3',4,4'-biphenyltetracarboxylic dianhydride
TeMPD	2,3,5,6-tetramethyl-1,4-phenylenediamine
mPD	1,3-phenylene diamine
IPDA	4,4'-(isopropylidene) dianiline

pressures. As noted in the references,[9–12] all permeation measurements were carried out with downstream under vacuum and low-pressure feed stream conditions, such that plasticization effects in these materials due to C_2H_4 and C_2H_6 are essentially nonexistent in the pressure range considered. Bickel and Koros[12] carried out pure gas C_2H_4 and C_2H_6 permeation measurements at 35°C up to 17 atm feed pressure and reported no upswing in permeability with pressure, indicating that no plasticization effects occurred. Similarly, Chan et al.[9,10] reported no occurrence of plasticization for C_2H_4 and C_2H_6 feed pressures up to 16 atm. These reported data for the pressure dependence of C_2H_4 and C_2H_6 permeability provide adequate evidence to claim that plasticization effects are minimal in the feed pressure range of 2–5 atm considered for the upper bound analysis.

Measurements on 6FDA-6FpDA have been reported by both Bickel and Koros[12] and Chan et al.[9]; however, the measurements have been reported at two different pressures. Based on the so-called "dual mode sorption and transport" effects, it is understandable that the C_2H_4 permeability is lower at a higher feed pressure. Additionally measurements on 6FDA—NDA have been reported by Chan et al.[9,10] at two different feed pressures, 2 atm and 5 atm, and again the permeability, as expected, is lower at the higher feed pressure. In order to keep the pressure range for the upper bound analysis as narrow as possible, we will consider the measurements for both 6FDA-6FpDA and 6FDA—NDA at the lower feed pressure, thus, making the pressure range for the analysis as 2–3.8 atm.

Three of the data points are based on measurements made as part of this work on polyimides Matrimid®, 6FDA-DAM and 6FDA:BPDA-DAM, details of which have already been mentioned in the previous sections. The chemical structures for the polymers are shown in Figure 2. Matrimid® 5218 (BTDA-DAPI), a commercially available polyimide, was purchased from Huntsman International LLC. 6FDA-DAM and 6FDA:BPDA-DAM were synthesized in-house following standard procedure.[24,25] Details of dense film casting and permeation measurements have been reported previously.[5,26,27]

It should be noted that one of the polymers tested in this work, 6FDA-DAM, has the same chemical structure as 6FDA-TrMPD tested by Tanaka et al.[11] classified under a different chemical name. Although there is some difference in the results reported here and by Tanaka et al.[11] the values reported are fairly close and can be considered equivalent within experimental uncertainty related to polyimide synthesis procedures, membrane formation, testing and measurement.

Some of the literature data have not been considered for the upper bound development. In 1992 Ilinitch et al.[28] reported C_2H_4 and C_2H_6 permeability and C_2H_4/C_2H_6 selectivity for poly(phenylene oxide) (PPO), two PPO-based copolymers and several rubbery polymers tested for a gas mixture containing 85 vol % CH_4,10 vol % C_2H_4 and 5 vol % C_2H_6. In a 1993 article the authors[29] published a corrigendum stating that due to a technical error, the permeabilities reported in 1992 were one-order of magnitude higher than the actual values. These results have not been included in the upper bound analysis since they are based on ternary gas mixtures, whereas all the data here considered are based only on pure gas measurements. In addition, in 1993 Ilinich et al.[29] reported results based on transient state permeation experiments for C_2H_4/C_2H_6 separation. These data have not been included in the upper bound analysis, which takes into account only steady-state permeation measurements. Teplyakov and Meares[30] reported permeability data for several rubbery and glassy polymers. These measurements were reported at 25°C and have not been considered in the upper bound analysis. In any case, the results do not affect the position of the upper bound line since the reported performances are quite low. For example, for PVTMS, a glassy polymer, the C_2H_4 permeability is 12 Barrer with C_2H_4/C_2H_6 selectivity of only 1.6.

Two different fits, based on the highest performance points on the plot, have been shown for the experimental upper bound line, drawn to aid the eye. Fit 1 spans 6FDA—NDA, 6FDA—NDA/durene (75:25) and 6FDA—NDA/durene (25:75), while fit 2 spans 6FDA—NDA/durene (75:25), 6FDA—NDA/durene (25:75) and 6FDA/BPDA-DAM (50:50). It should be noted that the experimental C_2H_4/C_2H_6 upper bound is defined here based on only a few polymers. This is, however, not so different from the upper bound for several other gas pairs (from He, H_2, O_2, N_2, CO_2 and CH_4) as defined by Robeson in 2008,[15] where only a few high-performing polymer materials lie at the upper bound line.

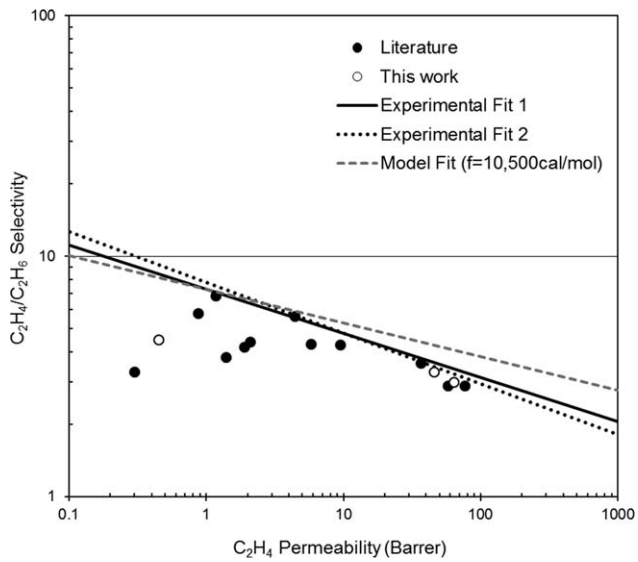

Figure 1. Plot showing C_2H_4/C_2H_6 data from Table 1 along with two fits for the experimental C_2H_4/C_2H_6 upper bound line drawn to aid the eye as well as the predicted C_2H_4/C_2H_6 upper bound line.

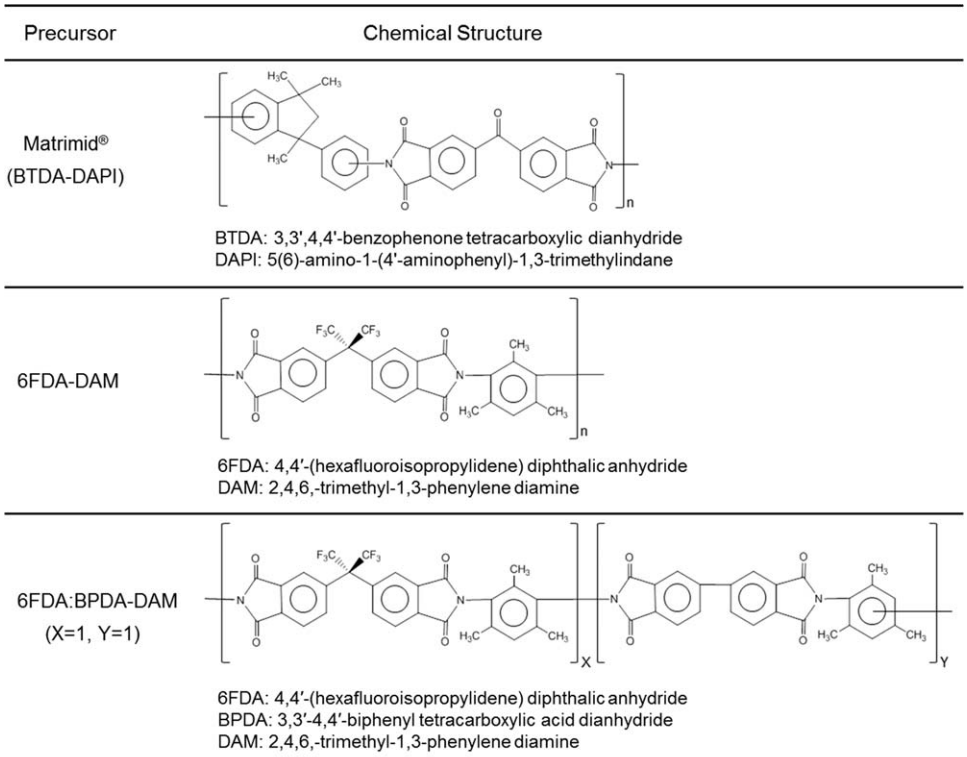

Figure 2. Chemical structures and chemical names of polymers used in this work.

Predicting the C_2H_4/C_2H_6 Upper Bound

The experimental upper bound shown in Figure 1 is based on high-performing 6FDA-based polyimides which are the current best in-class polymeric materials for such gas separations, and can, hence, be considered a good estimate of the tradeoff curve for C_2H_4/C_2H_6 separation. However, unlike the case of smaller gas pairs, since the sample space for consideration of the experimental C_2H_4/C_2H_6 upper bound is extremely limited, it is useful to consider modeling work in an effort to predict where the C_2H_4/C_2H_6 upper bound should lie.

As described earlier, a previous analysis by Freeman[16] provides a general quantitative description of the upper bound performance of polymeric membranes. Equations 6 and 7 presented previously can be used to estimate the slope (λ) and front factor (β) of the upper bound.

The slope, λ can be predicted with no adjustable parameters, and depends only on the size of the molecules, suggesting that the slope of the upper bound is a natural consequence of the sieving nature of stiff chain 6FDA-based glassy polymers that generally define the upper bound. In order to apply the analysis to C_2H_4/C_2H_6 separations, the first step is to represent the sizes of C_2H_4 and C_2H_6. The molecular size for low-molecular-weight penetrants permeating through polymer membranes is often represented by either its kinetic diameter (based on the minimum equilibrium cross-sectional diameters) determined using van der Waals length or the collision diameter calculated from the Lennard-Jones potential. For light gases, Freeman[16] used the kinetic diameters of the molecules given by Breck[31] to obtain λ, and the values are in good agreement with the upper bound slope as published by Robeson.[14] For small molecules (except CO_2) the difference between the kinetic and Lennard-Jones diameters are negligibly small. However, for higher hydrocarbons, the difference between the effective sizes can be significant and the kinetic diameter may no longer provide a reasonable size for the molecules.[23] Burns and Koros,[22] hence, used the Lennard-Jones diameter instead of the kinetic diameter for C_3H_6 and C_3H_8. Table 3 reports the size of C_2H_4 and C_2H_6 from different sources.

As in the case of C_3H_6/C_3H_8, we used the Lennard-Jones collision diameter as the most appropriate currently available representation of the sizes of C_2H_4 and C_2H_6 in order to predict the slope (λ) of the polymeric upper bound. It should be noted that while this is the best available representation of the sizes of C_2H_4 and C_2H_6 for transport through polymeric membranes and for the purpose of predicting the upper bound, the situation is more complex for molecular sieving materials like carbon molecular sieves (CMS).

Table 3. Size and Lennard Jones Temperature of C_2H_4 and C_2H_6 from Various Sources

	σ (Å)			ε/k (K)	
Source	C_2H_4	C_2H_6	Remarks	C_2H_4	C_2H_6
van Krevelen [21]	4.16	4.44	LJ collision diameter	225	216
Reid & Sherwood [91]	4.16	4.44	LJ collision diameter	224.7	215.7
Hirschfelder [92]	4.23	4.42	Viscosity measurements	205	230
Hirschfelder [92]	4.1	4.5	Four center model	-	-
Bickel & Koros [12]	3.7	4.1	Dreiding force field	-	-
Breck [31]	3.9	-	Molecular sieve	-	-

Thus, for C_2H_4/C_2H_6 transport in polymeric membranes and for the polymeric upper bound prediction, we take $d_A = 4.16$ Å and $d_B = 4.44$ Å (Table 3), and, from Eq. 6, the predicted upper bound slope is

$$\lambda_{A/B} = \left(\frac{d_B}{d_A}\right)^2 - 1 = 0.14$$

The front factor β for the upper bound can be predicted with only one adjustable parameter f using Eq. 7. In order to predict β from Eq. 7 we need to define an average sorption coefficient for C_2H_4 and the average C_2H_4/C_2H_6 sorption selectivity, as well as the value of f.

Penetrant sorption in polymers is governed by the condensability of the gas and its interactions with the polymer matrix.[16,21,23] In the absence of any significant polymer-penetrant interactions, the penetrant sorption is typically dominated mainly by its chemical nature and scales with convenient measures of the penetrant condensability, such as its boiling point, critical temperature, Lennard-Jones temperature, etc.[30,32] A general correlation between the sorption coefficient of a penetrant in amorphous polymers and the penetrant Lennard-Jones temperature ($\frac{\varepsilon_A}{k}$) can be represented from classical thermodynamics as follows[21]

$$\ln S_A = M + N\left(\frac{\varepsilon_A}{k}\right) \quad (9)$$

van Krevelen[21] reported values for M and N at 25°C for both rubbery and glassy polymers. Thus, a simple linear relationship between the sorption coefficients of various gases at 25°C in glassy polymers and their Lennard-Jones temperatures is given as

$$\log S\,(298) = -7.4 + 0.010\left(\frac{\varepsilon}{k}\right) \pm 0.6 \quad (10)$$

The sorption coefficient of gases in polymers follows a van't-Hoff type relation with temperature [21,33]

$$S(T) = S_o \exp\left(-\frac{H_S}{RT}\right) \quad (11)$$

where, S_o represents the front factor for sorption and H_s represents the heat of sorption.

van Krevelen also presented a simple linear relationship between the heat of sorption for a gas in a glassy polymer and its Lennard-Jones temperature[21]

$$10^{-3}\frac{\Delta H_S}{R} = 0.5 - 0.010\left(\frac{\varepsilon}{k}\right) \pm 1.2 \quad (12)$$

Equations 10, 11 and 12, thus, allow us to obtain average sorption values for ethylene and ethane in glassy polymers at 35°C, the temperature considered for the upper bound analysis, as follows

$$\log S\,(T) = \log S\,(298) - 0.435\left(\frac{\Delta H_S}{R}\right)\left(\frac{1}{T} - \frac{1}{298}\right) \quad (13)$$

The average C_2H_4 sorption coefficient and C_2H_4/C_2H_6 sorption selectivity values at 35°C as obtained from Eq. 13 are as follows

$$S_{C2H4} = 0.008\left(\frac{cm^3(STP)}{cm^3(polymer)\,cmHg}\right)$$

$$\frac{S_{C2H4}}{S_{C2H6}} = 1.2$$

where 1 $cm^3/[cm^3.cmHg] = 0.75$ $m^3/[m^3.kPa]$.

In all following discussions, figures and tables, 1 $cm^3(STP)/cm^3$ (polymer) has been abbreviated as 1 cm^3/cm^3 for convenience.

We also considered the experimental sorption data for C_2H_4 and C_2H_6 from literature.[9–12] Owing to the lack of tabulated data in some cases, some of the data points were read directly off the plots and may thus be approximate. Additionally we measured sorption isotherms for Matrimid®, 6FDA-DAM and 6FDA:BPDA-DAM using methods described elsewhere.[34,35] The sorption isotherms of Matrimid®, 6FDA-DAM and 6FDA:BPDA-DAM are shown in Figure 3. The experimental sorption data is compiled in Table 4.

The sample space for the average experimental sorption values is limited and does not span the entire range of the upper bound. Additionally the data available are at different temperatures and pressures, and the sorption values reported in Table 4 are at the same temperature and pressure as the corresponding permeability values reported in Table 1. While such effects are somewhat suppressed in the overall permeability due to the counteracting behavior of the sorption and diffusion coefficients, the effect when focused on sorption alone may be significant. The experimental sorption value may still give a reasonable estimate of the C_2H_4/C_2H_6 upper bound; however, owing to insufficient experimental data we focus on the theoretical averages for prediction of the upper bound.

The only adjustable parameter in predicting β is f, a parameter relating the activation energy for diffusion to the square of the penetrant diameter as follows[36]

$$E_{DA} = c d_A^2 - f \quad (14)$$

where c and f depend on the polymer. The value of f ranges from zero for rubbery polymers and low-performance glassy polymers to 14,000 cal/mol for the polyimide prepared by Haraya et al.[17] Freeman[16] used a value of $f = 12{,}600$ cal/mol based on a best fit of the model predictions to Robeson's upper bound[14] for several light gas pairs. Here we vary f from 10,000—14,000 cal/mol in order to predict the theoretical C_2H_4/C_2H_6 upper bound and compare it with the experimental upper bound.

Figure 1 shows the predicted upper bound for a value of $f = 10{,}500$ cal/mol against the experimental upper bound. All of the experimental data points lie below the predicted upper bound line. The values of λ and β obtained from the theoretical prediction as well as those obtained for the experimental upper bound are summarized in Table 5.

Clearly, a value for $f = 10{,}500$ cal/mol furnishes a very good agreement between the predicted C_2H_4/C_2H_6 upper bound and experimental fit 1.

Advanced Membranes for C_2H_4/C_2H_6 Separations

Although some polymeric materials, including high-performing 6FDA-based polyimides have been tested for the separation of olefin/paraffin mixtures, rather low permeabilities or selectivities were obtained as shown previously. This is a consequence of the similar molecular sizes and solubilities of C_2H_4 and C_2H_6, hence, resulting in poor separation performance. The upper bound tradeoff indicates that for polymeric membranes, C_2H_4/C_2H_6 selectivity over 10 may only be achieved for extremely low C_2H_4 permeability < 0.5 Barrer. On the other hand, for C_2H_4 permeability over 10 Barrer, selectivity cannot exceed 6. In addition to this undesired tradeoff, polymeric membrane stability under aggressive, high-pressure hydrocarbon feed stream conditions can

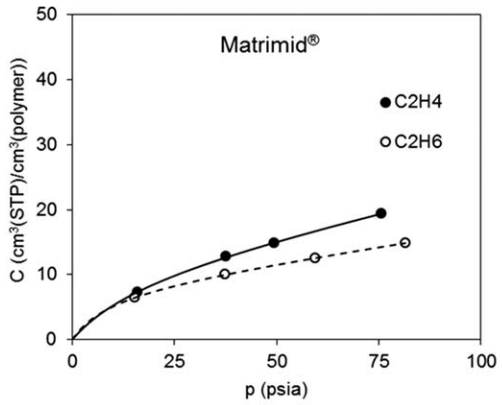

Matrimid®			
		C_2H_4	C_2H_6
C'_H	[cm³/cm³]	11.1	8.2
b	[1/psia]	0.054	0.104
k	[cm³/(cm³.psia)]	0.139	0.092

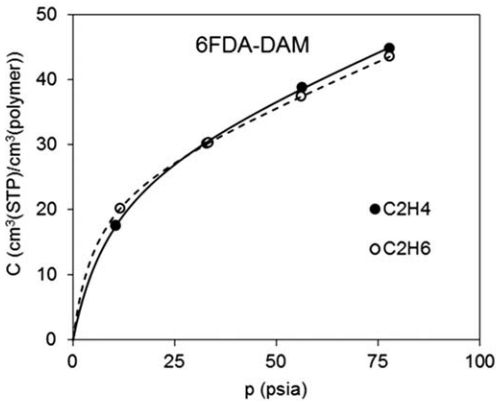

6FDA-DAM			
		C_2H_4	C_2H_6
C'_H	[cm³/cm³]	29.0	25.3
b	[1/psia]	0.101	0.184
k	[cm³/(cm³.psia)]	0.248	0.256

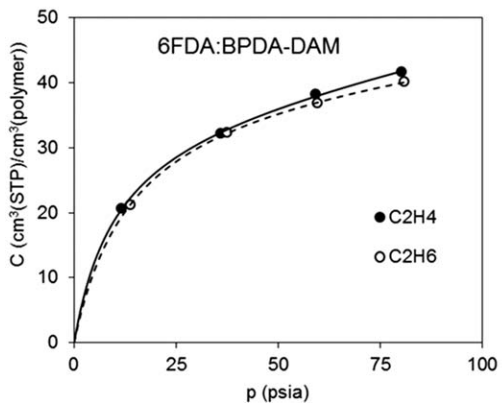

6FDA:BPDA-DAM			
		C_2H_4	C_2H_6
C'_H	[cm³/cm³]	35.6	40.8
b	[1/psia]	0.099	0.073
k	[cm³/(cm³.psia)]	0.127	0.065

Figure 3. C_2H_4 and C_2H_6 sorption isotherms for Matrimid®, 6FDA-DAM and 6FDA:BPDA-DAM at 35°C (1 cm³/cm³ = 1 m³/m³, 1 psia = 6.895 kPa, 1 cm³/[cm³.psia] = 0.145 m³/[m³.kPa]).

be a serious issue, with plasticization and selectivity loss occurring even for the most rigid polymer membranes. Because of these concerns, significant research has been directed toward developing more advanced membranes for olefin/paraffin separations.

The theory essentially implies that there are two ways to overcome the polymeric upper bound (1) by increasing the sorption selectivity of the membrane material toward C_2H_4, and (2) by increasing the sieving capability of the membranes to enhance the C_2H_4/C_2H_6 diffusion selectivity. The sections *Facilitated Transport Membranes* and *Molecular Sieve Membranes,* respectively discuss these two approaches

Table 4. Experimental C_2H_4 and C_2H_6 Sorption Data for Polymers

Precursor	T °C	P Atm	S_{C2H4} cm³/(cm³.cmHg)[a]	S_{C2H4}/S_{C2H6}	Source
6FDA-1,5-NDA	35	5.0	0.085	1.10	9
6FDA-TrMPD	50	2.0	0.150	1.00	10
6FDA-6FpDA	35	3.8	0.125	1.12	12
Matrimid®	35	3.4	0.058	1.30	This
6FDA-DAM	35	3.4	0.140	1.03	work
6FDA:BPDA-DAM	35	3.4	0.138	1.02	
Average			0.116	1.10	

[a]1 cm³/[cm³.cmHg] = 0.75 m³/[m³.kPa]

Table 5. Slope and Front Factor Values for C_2H_4/C_2H_6 Upper Bound

	$\lambda_{C2H4/C2H6}$	$\beta_{C2H4/C2H6}$ (Barrer)$^{\lambda}$
Theoretical Prediction	7.3	0.14
Experimental Fit 1	7.3	0.18
Experimental Fit 2	7.8	0.21

Table 6. C_2H_4/C_2H_6 Separation Performance for Different Types of Facilitated Transport Membranes[38,42]

Class	Membrane type	Carrier	P_{C2H4}	P_{C2H4}/P_{C2H6}	Source
			Barrer		
SLM	PEO	$AgNO_3$	1200	290	93
	Cellulose filter	$AgNO_3$	-	1000	93
ILM	Nafion	$AgBF_4$	400–700	30–400	94
	PS	$AgNO_3$	1800	200	95
FLM	PDMS/PPSQ	$AgNO_3$	28000	55	96
	PP	$AgNO_3$	1000	500	97
HFMC	SPEEK	$AgNO_3$	10000	2700	98
	SPEEK/SPEEK	$AgNO_3$	180	3800	98
Solid Electrolyte	PEO	$AgBF_4$	11.1	120	41
	CA	$AgBF_4$	-	10–280	99
	PVMK	$AgBF_4$	-	40–250	100

PEO- poly(ethylene oxide); PS- polysulfone; PP- polypropylene; CA- cellulose acetate; PVMK- poly(vinyl methyl ketone); SPEEK- sulfonated poly(ether ether ketone);
PDMS/PPSQ- polydimethylsiloxane/polyphenylsilsesquioxane

and advanced membranes that are capable of overcoming the polymeric C_2H_4/C_2H_6 upper bound.

Facilitated Transport Membranes. The average C_2H_4/C_2H_6 sorption selectivity for polymeric membranes is close to ~1.2. In theory, increasing the sorption selectivity of C_2H_4 over C_2H_6 in the membrane material can lead to enhanced overall selectivity surpassing the upper bound. This could be achieved by functionalizing the membrane materials with groups or ions that preferentially interact with C_2H_4 over C_2H_6, thus, increasing C_2H_4 uptake. Facilitated transport membranes have attracted research interest because of their potential to achieve this favorable sorption selectivity. In a facilitated transport process, passive diffusion across a concentration gradient is supplemented by the presence of a carrier agent that selectively and reversibly binds with a desired component targeted for separation, enhancing its transport across a barrier. Metal salts, such as those of silver, copper, etc., present as the carrier agent in the membrane, form electron donor/acceptor complexes with olefins (in this case C_2H_4) through interactions of the olefin π-orbitals with the metal ion, thus, enhancing their movement across the membrane. While the exact mechanism for transport of olefins across the membrane by complexation is complex, it has been suggested that facilitated transport occurs by either mobile diffusion of the Ag^+-solute complex through the membrane or by movement of the olefin across fixed silver sites by a hopping mechanism.[3,37,38]

In principle, facilitated transport membranes are capable of achieving exceptional selectivity for C_2H_4 over C_2H_6, capable of transcending the upper bound. Such membranes have been investigated by several researchers.[3,37–41] A comprehensive review on olefin/paraffin separation using facilitated membranes has been presented by Azhin et al.[42] and more recently by Faiz and Li.[38] However, although the starting performance of facilitated transport membranes (see Table 6) is far beyond the polymeric C_2H_4/C_2H_6 upper bound, the membranes typically degrade rapidly with large performance losses, thus making them questionable for practical application.[37,38]

Facilitated liquid membranes consist of a microporous membrane either impregnated with a solution carrier or with a continuously circulated carrier liquid stream. Liquid membranes have been investigated in several different configurations such as immobilized liquid membranes (ILM), both supported (SLM) and ion-exchanged (IEM), flowing liquid membranes (FLM), and hollow fiber membrane contactors (HFMC), etc.[38] Facilitated liquid membranes, however, show rapid performance loss resulting from several drawbacks such as carrier loss, gas-liquid contact, membrane wetting, etc.[38]

Membrane electrolytes are a more recent class of facilitated transport membranes which do not use liquids as facilitation carriers; instead olefin transport occurs in the solid state.[37,38,41] They are composed of metal salts dissolved in the polymer matrix, where both anions and cations are sufficiently mobile without the need of a solvent to promote ionic motion and conductivity. Unlike liquid membranes, these polymer electrolyte membranes can sustain higher pressure difference across the membrane without physical loss of the complexing agent, and can be operated with dry feeds. However, long-term chemical stability is an issue, with decline in the membrane performance occurring due to reduction of silver ions to silver nanoparticles and other silver compounds. Silver ions can be reduced in the presence of light. In addition, impurities present in the feed stream such as H_2, H_2S, and C_2H_2, etc., can poison the carrier ions, thus, degrading the membranes. Once the membrane is degraded, regeneration is not very practical.[37,38] Further jeopardizing the performance of membrane electrolytes is a recently reported phenomenon called olefin-conditioning.[37] Electrolyte membranes are not stable even in the presence of ideal C_2H_4/C_2H_6 mixtures, and it has been shown that over time the presence of an olefin (C_2H_4), which can complex with silver ions, irreversibly alters and degrades the membrane. Over time, a decrease in the C_2H_4 flux is the primary cause for selectivity decline. To date, an effective strategy to mitigate the effect of "olefin conditioning" has not been identified.[37]

Facilitated transport membranes, therefore, still present a large challenge in improving the stability of the olefin complexing agent to develop membranes with lifetimes satisfactory for commercial application. Significant fundamental research and perhaps even the development of a breakthrough, intrinsically stable carrier may be required for making facilitated transport membranes practical for industrial implementation.

Molecular Sieve Membranes. A second approach to overcome the polymeric upper bound is to increase the sieving capability of membranes which will in turn increase the C_2H_4/C_2H_6 diffusion selectivity. Over time, increasing polymer chain rigidity while simultaneously increasing interchain spacing, for example by introducing packing-inhibiting bulky groups and intrinsically rigid linkages, has pushed the upper bound for several gas pairs.[15] Nevertheless, polymers cannot achieve a true molecular sieving effect owing to flexible chains, and pushing the sieving capability of solution processable polymers by tailoring their structure may have reached its limits.

Materials such as zeolites, metal organic frameworks (MOFs) including zeolitic imidazolate frameworks (ZIFs), carbon molecular sieves (CMS), etc., on the other hand consist of rigid pore structures with arrays of channels of molecular dimensions which can offer the possibility of size and shape selective separations, and are, thus, capable of surpassing the polymeric upper bound.[43]

Crystalline Molecular Sieve Membranes. Most studies relating to C_2H_4/C_2H_6 separation using crystalline molecular

sieves have focused on cyclic batch adsorption/desorption type processes, but in principle, a steady-state membrane process can be a more attractive alternative.[44] Enriching C_2H_4 from C_2H_4/C_2H_6 mixtures is truly one of the most challenging separations as evidenced by the incapability of small pore eight-ring zeolitic molecular sieves, such as zeolite NaA, CHA, AlPOs, SAPOs, and DD3R to discriminate C_2H_4 and C_2H_6 molecules on the basis of size selectivity.[45–47] These eight-ring zeolitic molecular sieves, which are considered to be the most size-selective crystalline molecular sieves, have been shown to be highly promising for C_3H_6/C_3H_8 with diffusion selectivity in the range of 10^3-10^5; however, can hardly separate C_2H_4 and C_2H_6 by a factor of more than 3 based on the differences in diffusion rates.

Adsorption of C_2H_4, in some cases, is drastically favored over C_2H_6 in alumina-rich cationic zeolites (e.g., zeolite A and X), and metal-organic frameworks (e.g., Fe_2(dobdc)) due to strong interactions between the C_2H_4 π-bond and adsorbents surfaces, which leads to a sorption selectivity in the range of 10–20.[46,48,49] Unfortunately, these promising selectivities are only achievable at very low-surface densities and diminish quickly as the feed pressure reaches atmospheric and saturation limits are approached. Therefore, for pure zeolite or MOF membranes with feed pressures higher than several atmospheres, the C_2H_4/C_2H_6 permselectivity are expected to be less than 5 in most cases, which is far from being commercially attractive.

Zeolitic imidazolate framework-8 (ZIF-8) belongs to the subfamily of MOFs with zeolite or zeolite-like topologies and has recently been extensively studied due to its interesting molecular sieving properties, promising for gas separations.[50–55] While ZIF-8 has been shown to be highly kinetically selective for C_3H_6 over C_3H_8 and n-C_4H_{10} over iso-C_4H_{10},[52] both computational and experimental studies have suggested that the C_2H_4/C_2H_6 selectivity in ZIF-8 is quite limited.[56–60] Pan and Lai[56] investigated ZIF-8 membranes for separation of hydrocarbon mixtures and their membranes show a pure component C_2H_4/C_2H_6 selectivity close to 2. ZIF-8 membranes fabricated by Caro and coworkers[60,61] showed an ideal C_2H_4/C_2H_6 selectivity of 4.2 for pure component feeds, and for an equimolar mixture of C_2H_4/C_2H_6 selectivity of 2.8 and 2.4, respectively, for 1 and 6 bar feed pressure were reported. This moderate C_2H_4 selectivity over C_2H_6 was explained by the interplay of a preferential C_2H_6 adsorption selectivity competing with preferential C_2H_4 diffusion selectivity.

Thus, zeolite or MOF/ZIF membranes have, thus, far not been shown to be able to deliver attractive C_2H_4/C_2H_6 selectivity. Figure 4 shows a plot of the C_2H_4/C_2H_6 separation performance of crystalline molecular sieves against the polymeric upper bound. Another limitation of using these pure zeolite or MOF/ZIF membranes is the expensive fabrication cost and their brittle nature, as well as difficulty in fabricating a sufficiently coherent and robust membrane on a large scale.

Mixed Matrix Membranes. Mixed matrix membranes, which are formed by dispersing molecular sieve particles/platelets in polymer matrices, are promising approaches for gas and vapor separations that combine the ease of processing polymers with the superior separation performance of molecular sieves.[62] Zeolite-based mixed matrix membranes pose challenges relating to adhesion at the polymer-sieve interface, which may make it hard to fabricate sufficiently

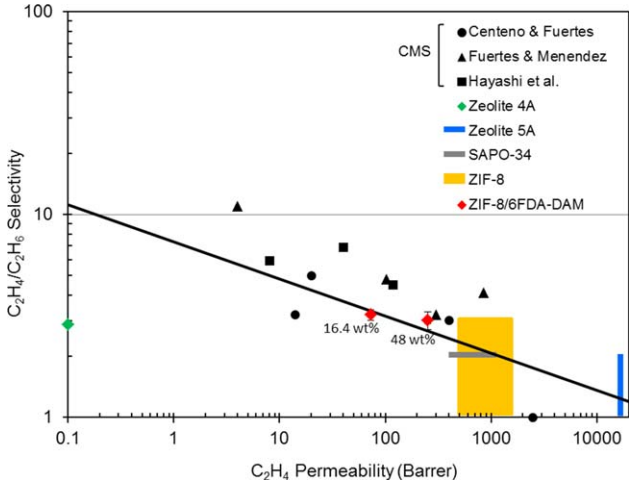

Figure 4. Plot showing C_2H_4/C_2H_6 separation performance of crystalline molecular sieves,[46,51,86–88] mixed matrix membranes[51,52] and carbon molecular sieve membranes[75,77,89] with respect to the polymeric C_2H_4/C_2H_6 upper bound line.

[Color figure can be viewed in the online issue, which is available at wileyonlinelibrary.com.]

coherent and defect-free membranes. On the other hand, MOFs/ZIFs are intrinsically more compatible with glassy polymers and their introduction has open up new opportunities for mixed matrix membranes. Figure 4 shows C_2H_4/C_2H_6 separation performance of mixed matrix membranes fabricated with polyimide 6FDA-DAM and ZIF-8. Contrary to the case of C_3H_6/C_3H_8 separation,[51] attractive C_2H_4/C_2H_6 selectivity has not been achieved with this platform. Maxwell model calculations showed that the C_2H_4/C_2H_6 permselectivity in ZIF-8 is unattractive,[52] which is generally consistent with permeation results of pure ZIF-8 membranes noted previously. Similarly unfavorable selectivities were also seen from mixed matrix membranes prepared with ZIF-8 and poly(1,4-phenylene ether-ether-sulfone).[63] More recently, it was reported that adding 20 wt % MOF (Cu_3BTC_2) particles into a P84 polyimide matrix would result in a C_2H_4/C_2H_6 permselectivity enhancement of 70% over the neat polyimide film, and the resulting mixed-matrix permselectivity was reported as 7.1.[64]

Carbon Molecular Sieve Membranes.

Carbon molecular sieve (CMS) membranes are formed from the high-temperature pyrolysis of polymer precursor membranes under controlled conditions.[5,65,66] They have shown the potential to outperform the polymeric upper bound for gas pairs such as O_2/N_2 and CO_2/CH_4.[43,67–69] The structure of CMS membranes is visualized to be made up of disordered sp^2-hybridized condensed hexagonal graphite-like sheets with pores formed from packing imperfections. They are amorphous materials with so-called "slit-like" pores,[70] and the ideal pore structure of such materials can be described as a combination of larger micropores ($\approx$ 6–20 Å) connected by smaller ultramicropores ($<$ 6 Å), resulting in a bimodal distribution. The ultramicropores in CMS membranes can discriminate between molecules of different size and shape allowing molecular sieving separation of penetrant molecules, and can be imagined to be analogous to the

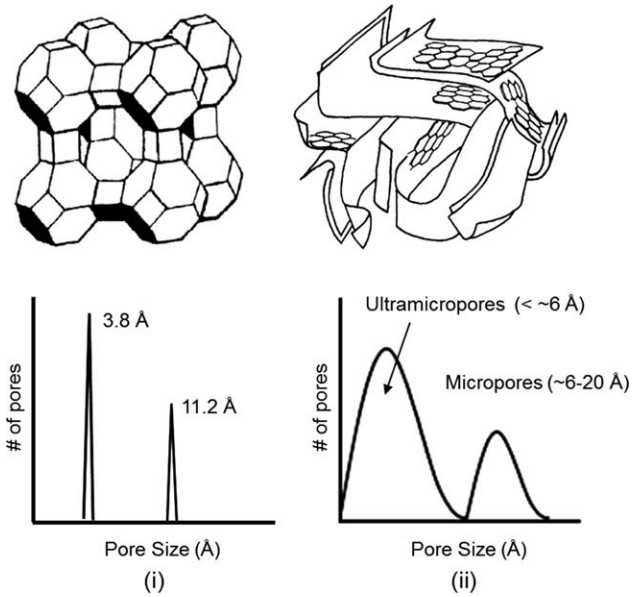

Figure 5. Schematic of the structure and pore-size distribution of (1) Zeolite 4A,[72] and (2) CMS membrane.[70,90]

limiting dimension of a zeolite cage window.[5,65,66,71] However, zeolites are crystalline materials consisting of a 3-D framework of $[SiO4]^{-4}$ and $[AlO4]^{-5}$ tetrahedra linked to form ordered structures of rings and cages with uniform, well-defined dimensions.[70,72] CMS membranes, on the other hand, are amorphous materials with a distribution of pore sizes that may be tuned by varying parameters such as the starting polymer precursor, pyrolysis conditions, etc.[5,73] Figure 5 shows a schematic representation of the structures and pore-size distribution in zeolite-4A and CMS materials.

An important feature distinguishing CMS from zeolites is that while zeolites and zeolite-like materials have a pore opening with a 2-D size restriction, the pore structure of CMS membranes is "slit-like"[73] with the pore opening having a 1-D size restriction. This allows CMS membranes a unique advantage in separating C_2H_4 from C_2H_6. C_2H_4 has a somewhat planar molecular configuration while C_2H_6 is bulkier in shape. The rigid "slit-like" CMS pores can very effectively discriminate between the subtle shape and configurational differences of C_2H_4 and C_2H_6, thus, enabling easy passage of the "slimmer" C_2H_4 while hindering several degrees of rotational freedom of the bulkier C_2H_6.[5,74] The zeolite pore opening cannot take advantage of the planar configuration of C_2H_4. From this perspective, CMS membranes should be somewhat theoretically ideal for C_2H_4/C_2H_6 separations. Figure 6 illustrates this concept.

C_2H_4/C_2H_6 separation using carbon molecular sieve (CMS) membranes has been studied by few researchers.[75–80] Fuertes and Menendez[75] prepared carbon membranes by carbonization (vacuum, 700°C) of a thin phenolic resin film deposited on the inner surface of an alumina tube support. They studied the effect of preoxidation and postoxidation in air on the separation characteristics of their membranes. In some cases, their carbon membranes were modified by

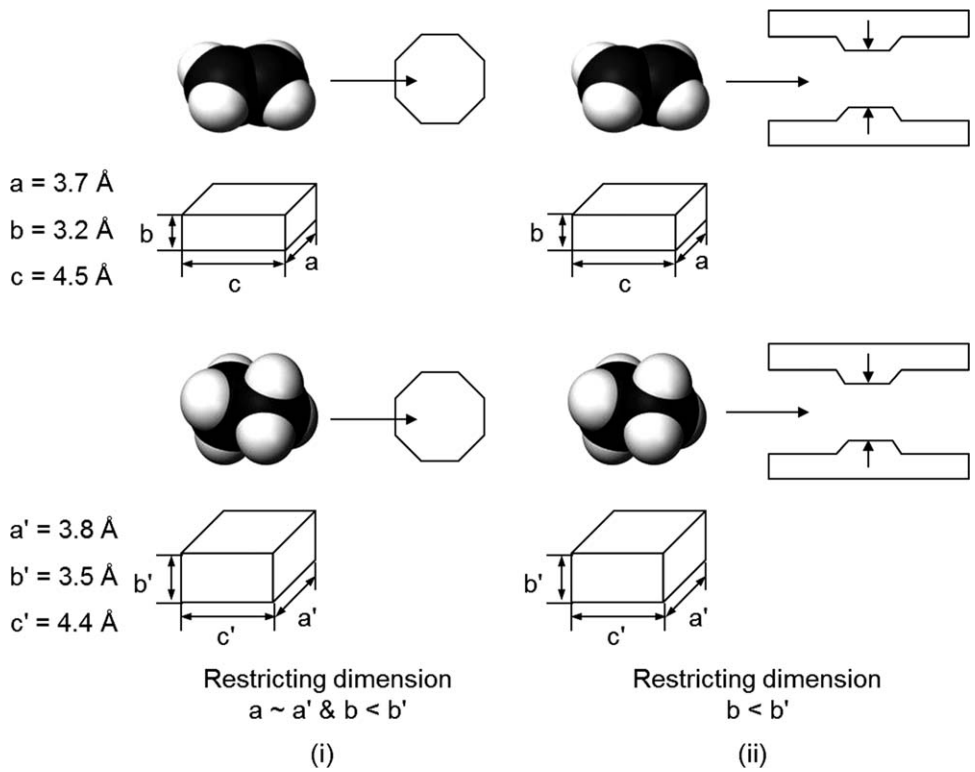

Figure 6. Illustration of the concept of the restricting dimensions for C_2H_4 and C_2H_6 in transport through (1) zeolites, and (2) CMS membranes.

The dimensions of C_2H_4 and C_2H_6 were obtained using space filling models. In a zeolite pore opening, the restricting dimensions for C_2H_4 and C_2H_6 transport are both $a \sim a'$ and $b < b'$, such that the limiting dimension (a and a') has 0.1 Å difference. For CMS membranes, the limiting dimension for C_2H_4 and C_2H_6 in the "slit-like" pore opening is $b < b'$, which has a 0.3 Å difference allowing greater diffusive advantage.

chemical vapor deposition (CVD) before or after air-oxidation. Their membranes show C_2H_4/C_2H_6 selectivity in the range of 1–11 depending on the treatment conditions. Similarly, Centeno and Fuertes[76] also fabricated CMS membranes by carbonizing a thin phenolic resin film deposited on the inner face of a ceramic tube. They studied the effect of varying different pyrolysis conditions such as the pyrolysis temperature, ramp rate, soak time and the pyrolysis atmosphere on their membranes. The C_2H_4/C_2H_6 selectivity they reported ranges from 0.97 (reverse selective) to ≈ 5. Hayashi et al.[77] prepared CMS membranes by carbonizing a BPDA-pp'ODA polyimide film formed on the outer surface of a porous alumina support in an inert argon stream at 700°C. Their membranes show C_2H_4/C_2H_6 selectivity between 4.4 and 6.9 depending on the number of coatings and the testing temperature. Okamoto et al.[80] prepared carbonized hollow fiber membranes by preoxidation and subsequent pyrolysis of a BPDA-based asymmetric hollow fiber precursor at temperatures of 500–700°C under nitrogen. Their membranes were studied primarily for C_3H_6/C_3H_8 and 1,3-butadiene/n-butane separation and showed a low C_2H_4/C_2H_6 selectivity of 3.1 with 600°C pyrolysis. The C_2H_4/C_2H_6 selectivity reported by Suda and Haraya[79] for CMS dense films fabricated via pyrolysis of polyimide Kapton at 1000°C under vaccum and further calcination at 400°C is ≈ 5. The CMS C_2H_4/C_2H_6 separation performance from literature is shown against the polymeric upper bound in Figure 4. Clearly CMS membranes show the ability to outperform the polymeric upper bound.

Carbon Molecular Sieve Membrane Processing

As discussed in the previous section, few researchers have investigated C_2H_4/C_2H_6 separation using CMS membranes, and CMS show the potential to surpass the polymeric upper bound. However, the membranes were generally not specifically developed for C_2H_4/C_2H_6 separation. Additionally, the drawback for the carbon membranes reviewed above is that in most cases the CMS membrane fabrication either involved multiple processing steps, which add to complexity and cost; or were formed on supports, which could not only be expensive but may also involve issues such as not being able to coherently fabricate a thin, defect free CMS membrane. The focus in this study is to establish a convenient, potentially scalable CMS membrane formation technology for C_2H_4/C_2H_6 separation, based on a method for optimizing performance by tuning the pyrolysis process alone, without any additional steps.

In fact one of the biggest advantages that CMS membranes can offer over other inorganic membranes is that CMS membranes may be relatively easily fabricated into defect-free membranes by directly pyrolyzing polymeric membranes under controlled conditions. Furthermore, their performance can be very effectively optimized by tuning several parameters such as the starting material and the pyrolysis conditions, including the final pyrolysis temperature, heating protocol and the pyrolysis atmosphere. While polymer membranes are the state of art technology, CMS membranes can also be relatively easily fabricated into realistic hollow fiber modules. The only additional step beyond the current technology platform is the scale-up of pyrolysis. Recently, Karvan et al[81] demonstrated the scale-up of a bench-scale CMS production system, consisting of a horizontal furnace setup and limited to a few fibers in one run, to a larger pilot-scale system with a vertical furnace for hundreds of fibers per pyrolysis cycle. This feature makes CMS membranes attractive for delivering high-separation performance not just from a materials perspective, but also from a commercial viability perspective.

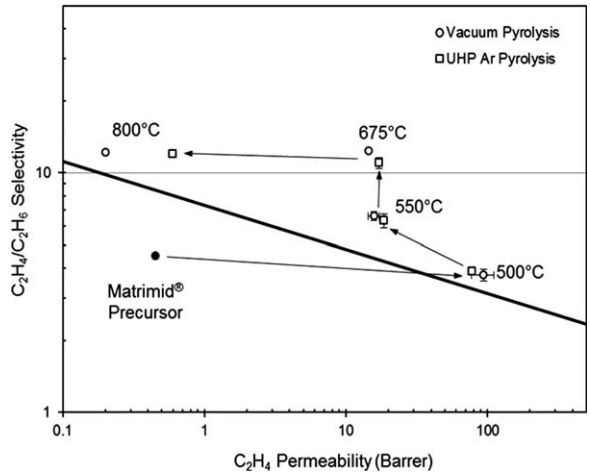

Figure 7. Plot showing C_2H_4/C_2H_6 separation performance (35°C, 50 psia, pure gas) of CMS dense films derived from vacuum pyrolysis and UHP Ar pyrolysis of Matrimid® at different pyrolysis temperatures.

Error bars represent standard deviations from multiple measurements.

CMS Membranes Derived from Matrimid®. Recently we reported the C_2H_4/C_2H_6 separation performance of free-standing CMS dense films fabricated by pyrolyzing a commercial polyimide Matrimid®[5] Details of CMS fabrication and permeation measurements have been described previously.[5] We reported performance optimization achieved by way of tuning the final pyrolysis temperature and heating rates during pyrolysis. The results were reproducible under both vacuum and inert, ultra-high purity (UHP) argon (Ar) pyrolysis conditions. This is especially important from a scalability aspect, since pyrolysis under inert gas would be practically preferred over vacuum pyrolysis. The key results for CMS obtained from Matrimid® pyrolysis using the heating protocol described below is reported in Figure 7. This method yielded an optimum C_2H_4 permeability $\approx$ 14–17 Barrer and C_2H_4/C_2H_6 selectivity $\approx$ 11–12 combination at a pyrolysis temperature of 675 °C.

Pyrolysis Heating Protocol

50°C→250°C at a ramp rate of 13.3°C/min
250°C→(T_{max}−15) °C at a ramp rate of 3.85 °C/min
(T_{max}−15) ° → T_{max} °C at a ramp rate of 0.25°C/min
Soak for 2 hours at T_{max}

where, T_{max} represents the final pyrolysis temperature.

Furthermore, the CMS membranes were also fabricated in the hollow fiber configuration by Xu et al.[82] by pyrolyzing Matrimid® hollow fibers, and the C_2H_4/C_2H_6 selectivity in the hollow fiber form were shown to be consistent with the dense films for all pyrolysis temperatures.[82]

CMS Membranes Derived from 6FDA:BPDA-DAM. While a convenient CMS membrane formation technique for C_2H_4/C_2H_6 separation was demonstrated in these previous works,[5,82] one of the disadvantages of using Matrimid® is

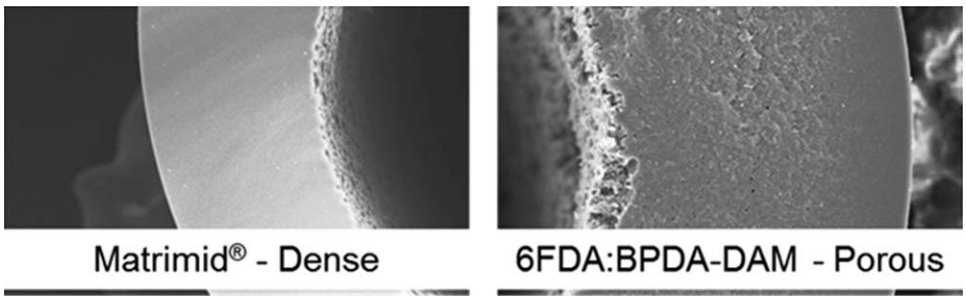

Figure 8. Morphology of Matrimid® and 6FDA:BPDA-DAM based CMS hollow fibers.[74]

that in the hollow fiber configuration the porous substructure of the polymer precursor hollow fiber collapses due to intensive heat treatment during the pyrolysis process.[82] As shown by Xu et al.[82] this substructure collapse leads to an increased separation layer thickness in the CMS hollow fiber, resulting in a drastic loss in the C_2H_4 flux. Consideration of the membrane flux is important from a practical perspective, since it is directly related to the membrane area and cost. Hence, in order to avoid low-flux resulting from this substructure collapse problem in the hollow fiber form, a new polymer precursor 6FDA:BPDA-DAM (see Figure 2) was investigated for CMS fabrication. Unlike Matrimid®, 6FDA:BPDA-DAM does not show severe substructure collapse and can retain some of its porosity after pyrolysis, as reported by Xu et al.[74] This is illustrated in Figure 8.

Additionally, 6FDA:BPDA-DAM has a higher fractional free volume compared to Matrimid® due to the presence of bulky $-CF_3$ groups in the polymer that hinder polymer chain packing (Figure 2). Hence, the intrinsic permeability of the 6FDA:BPDA-DAM is higher than that of Matrimid® in the polymeric membrane form. Conventional wisdom holds that CMS membranes fabricated from a precursor with higher fractional free volume generally results in CMS with higher permeability.[70,73] Additionally, the pyrolysis of 6FDA:BPDA-DAM results in the evolution of bulky CHF_3 components besides CO, CO_2 and CH_4 evolved during Matrimid® pyrolysis, which gives it a more open structure compared to CMS derived from Matrimid®[83] Hence, 6FDA:BPDA-DAM was investigated as a new starting precursor for CMS membrane fabrication for C_2H_4/C_2H_6 separation, and a method for tailoring the performance CMS derived from 6FDA:BPDA-DAM dense films by tuning the pyrolysis conditions is reported here.

As shown in the case of Matrimid®, the pyrolysis temperature is an effective tool in tuning CMS properties. Hence, the final pyrolysis temperature was used as the first tool to tune the performance of CMS derived from 6FDA:BPDA-DAM as well. The C_2H_4/C_2H_6 separation performance of CMS derived from UHP Ar pyrolysis of 6FDA:BPDA-DAM dense films at different final pyrolysis temperatures using the heating protocol reported earlier is shown in Figure 9. As seen in the case of Matrimid® an increase in the final pyrolysis temperature resulted in an increase in the C_2H_4/C_2H_6 selectivity and a decrease in permeability of the 6FDA:BPDA-DAM CMS. The 6FDA:BPDA-DAM CMS permeability is, however, much higher than the Matrimid® CMS permeability, at all pyrolysis temperatures, despite its somewhat lower selectivity. It is important to point out that although the general trends may be similar for Matrimid® and 6FDA:BPDA-DAM, the effect of final pyrolysis temperature on CMS properties is clearly precursor dependent.

The higher permeability of the 6FDA:BPDA-DAM CMS also allowed us to use a method to tune its performance based on the amount of oxygen present in the inert gas during pyrolysis. This method is called "oxygen-doping", and was originally developed by Kiyono et al.[68] for CO_2/CH_4 separation using CMS membranes. The presence of trace amounts of oxygen in the inert gas during pyrolysis allows tuning of the CMS performance by selective chemisorption of oxygen at high temperatures at the CMS ultramicropore sites that are believed to be $\approx$17 times more reactive than the basal plane.[68,84] This concept is illustrated in Figure 10. The use of oxygen-doping at a given pyrolysis temperature, thus, allows enhancement of the CMS selectivity by ultramicropore tuning up to a certain optimum oxygen level. Beyond this optimum, excess oxygen may result in performance loss as a result of CMS pore clogging due to "overdoping".[68] In this work, oxygen doping using 30 and 50 ppm oxygen in argon purge gas during pyrolysis was used at 550, 600 and 675°C to tune the C_2H_4/C_2H_6 separation performance of CMS derived from 6FDA:BPDA-DAM.

Additionally, a "postoxygen-doping", called "dual temperature secondary oxygen doping"[85] method using 30 and 50 ppm oxygen in argon was also used as another tuning parameter for 6FDA:BPDA-DAM CMS performance. The difference between "oxygen-doping" and "postoxygen-doping" is as follows: For oxygen-doping, pyrolysis is carried out for

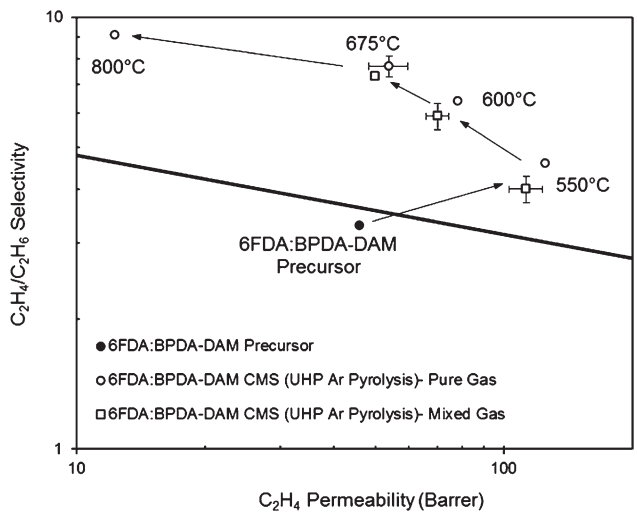

Figure 9. Plot showing C_2H_4/C_2H_6 separation performance (35°C, 50 psia) of CMS dense films derived from UHP Ar pyrolysis of 6FDA:BPDA-DAM at different pyrolysis temperature.

Error bars represent standard deviations from multiple measurements.

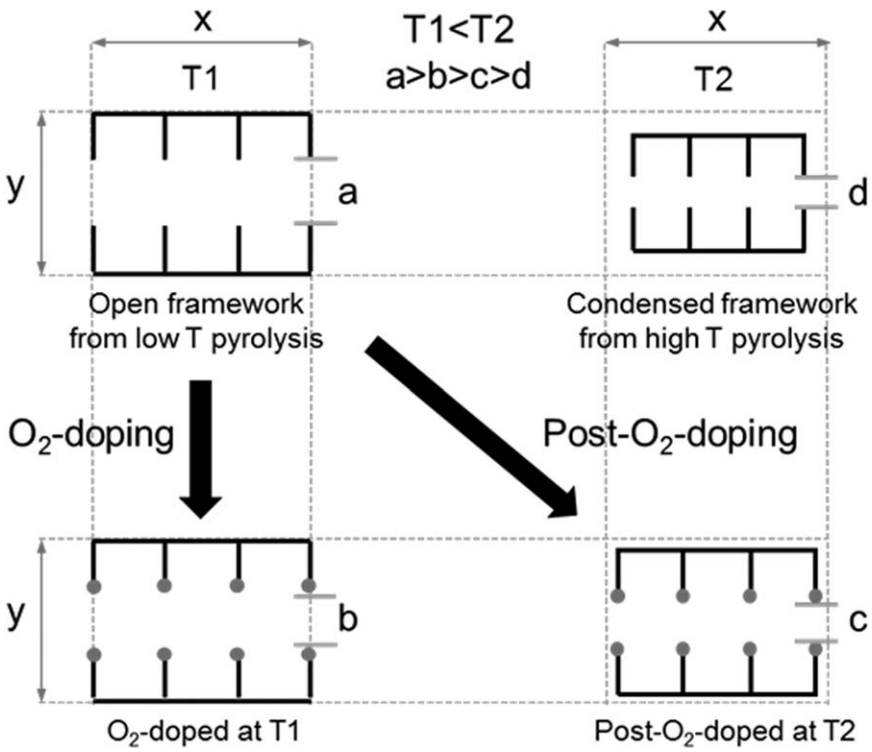

Figure 10. Schematic representation of the effects of final pyrolysis temperature, oxygen-doping and postoxygen-doping on CMS cartoon structures.

the entire pyrolysis cycle in the presence of inert purge gas containing trace concentrations of oxygen. By comparison, for postoxygen-doping, the CMS structure is first derived by pyrolysis at the final pyrolysis temperature in the presence of UHP argon. Thereafter, the fabricated CMS is quickly heated back up to a temperature higher than the final pyrolysis temperature in the presence of inert gas containing trace oxygen. This "secondary" step is called postpyrolysis as it occurs after the actual CMS formation via pyrolysis. Since oxygen-doping occurs during this secondary post pyrolysis step as opposed to during pyrolysis, the process is termed as "postoxygen-doping" or "dual temperature secondary oxygen doping."[85] The pyrolysis heating protocol described above was used for pyrolysis in all cases. The protocol listed below was used for postoxygen-doping CMS derived from UHP argon pyrolysis.

Postoxygen-doping protocol:

1. 50 °C→T_{post} at a ramp rate of 10 °C/min
2. Soak for 15 min at T_{post}

where, T_{post} is the temperature to which the CMS is heated in post pyrolysis, and postpyrolysis temperature (T_{post}) > pyrolysis temperature.

Figure 10 shows a comparison of the effects of final pyrolysis temperature, oxygen doping and post oxygen doping on the CMS cartoon structures.

As seen from Figure 10, pyrolysis at a lower pyrolysis temperature T1 results in an open intrinsic CMS framework. For oxygen-doping during pyrolysis at T1, the intrinsic open framework may not condense but the ultramicropores are tuned by selective chemisorption of oxygen at the ultramicropore (smaller pore window) sites. During pyrolysis at a higher pyrolysis temperature T2, the CMS framework is extensively condensed compared to CMS derived from T1 pyrolysis. When oxygen-doping is carried out during pyrolysis at T2, ultramicropore tuning occurs on this condensed CMS framework. By difference, for postoxygen-doping, the CMS is first derived at T1, thus, resulting in an open intrinsic starting framework. Next as the CMS is quickly heated up to a higher temperature T2 in the presence of oxygen during post-pyrolysis oxygen doping, there may be very little condensation of the CMS framework along with ultramicropore tuning resulting from oxygen chemisorption, as opposed to exaggerated condensation from slow heating during pyrolysis at T2. Thus, post-oxygen-doping allows another tool for tuning CMS performance. It can essentially take advantage of the combined effects of oxygen-doping and higher temperature, however, the resulting effects of both may be milder compared to oxygen doping or pyrolysis at higher temperature.

The following cases were studied (1) oxygen-doping: pyrolysis at 550°C and 600°C in 30 and 50 ppm O_2/Ar, pyrolysis at 675°C in 30 ppm O_2/Ar, and (2) postoxygen-doping: pyrolysis at 550°C in UHP Ar followed by post pyrolysis at 600°C in 30 and 50 ppm O_2/Ar, pyrolysis at 600°C in UHP Ar followed by post pyrolysis at 650°C in 30 ppm O_2/Ar. The results of oxygen-doping and post-oxygen doping are shown in Figure 11.

At all pyrolysis temperatures, oxygen-doping at 30 ppm resulted in C_2H_4/C_2H_6 selectivity increase along with C_2H_4 permeability loss. In going from 30 ppm to 50 ppm, the selectivity enhancement is not significant but further permeability loss occurs. This may be a result of "over-doping", as noted previously. Oxygen-doping depends on the final pyrolysis temperature. The effects of oxygen-doping on selectivity are much more significant at a lower pyrolysis temperature. With increase in the final pyrolysis temperature, the selectivity enhancement becomes less obvious while the permeability continues to decrease. This is related to the fact that the

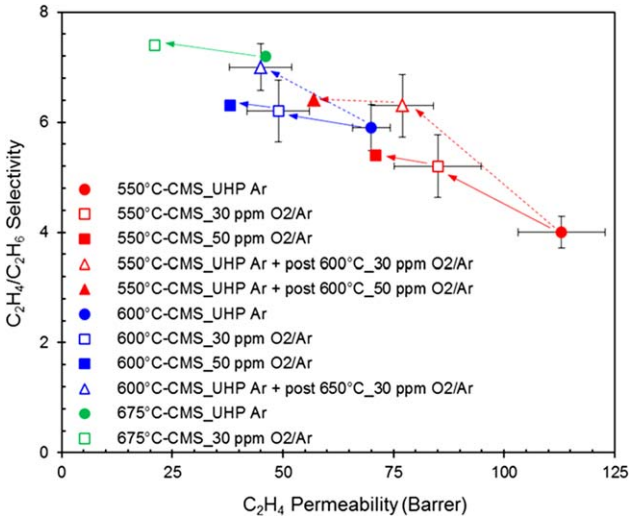

Figure 11. Effects of oxygen-doping and postoxygen-doping on the C_2H_4/C_2H_6 separation performance (35°C, 50 psia, 63.2 mol % C_2H_4 + 36.9 mol % C_2H_6) of CMS derived from 6FDA:BPDA-DAM.

Error bars represent standard deviations from multiple measurements. [Color figure can be viewed in the online issue, which is available at wileyonlinelibrary.com.]

"closed" CMS framework at a higher pyrolysis temperature allows less room for ultramicropore tailoring via oxygen-doping.

Post-oxygen-doping shows an improvement in C_2H_4/C_2H_6 selectivity over the undoped or oxygen-doped CMS for both pyrolysis temperatures, as seen from Figure 11. For CMS derived from 550°C UHP Ar pyrolysis, post-oxygen-doping at 600°C using 30 ppm O_2/Ar shows improved selectivity over both 550°C—CMS_30 ppm O_2/Ar and 550°C—CMS_50 ppm O_2/Ar. In fact, when compared to 600°C—CMS_UHP Ar, the postoxygen-doped CMS shows a higher permeability, yet comparable selectivity. In increasing the oxygen amount from 30 to 50 ppm during postoxygen-doping, the permeability decreases drastically with no increase in selectivity, which is likely the outcome of "over-doping". For CMS derived from 600°C UHP Ar pyrolysis, post treatment at 650°C using 30 ppm O_2/Ar still shows performance improvement over the 600°C—CMS_30 ppm O_2/Ar and 600°C_50 ppm O_2/Ar CMS. Although the standard deviations for multiple measurements must be considered, the C_2H_4/C_2H_6 performance trends from oxygen doping and post oxygen doping can be noticed from the aforementioned studies. These tools can, thus, be used for effective performance optimization depending on the end goal.

Conclusions

This article summarizes the C_2H_4/C_2H_6 separation performance using polymeric membranes, and presents an experimental C_2H_4/C_2H_6 upper bound for solution-processable polymeric membrane materials based on literature data. A theoretical prediction of the C_2H_4/C_2H_6 polymeric upper bound is also presented, and it shows good agreement with the experimental upper bound. The article further discusses two ways to overcome the polymeric ethylene/ethane upper bound, based on increasing the sorption or diffusion selectivity, and presents a review on advanced membrane types such as facilitated transport membranes, zeolite and metal organic framework (MOF) or zeolite imidazolate framework (ZIF) based membranes, and carbon molecular sieve membranes. The intrinsic instability of facilitated transport membranes makes them questionable for practical application. While membranes based on crystalline molecular sieves such as zeolites and MOFs can achieve very attractive propylene/propane separation, their C_2H_4/C_2H_6 performance generally remains below the polymeric upper bound. In addition, they may present challenges such as difficulties in coherently fabricating a defect-free membrane. Carbon membranes have shown the potential to surpass the polymeric C_2H_4/C_2H_6 upper bound performance. The main advantage of CMS membranes is that they can be based directly on the polymeric membrane platform, with pyrolysis being the only additional step in CMS fabrication. A convenient, potentially scalable method for tailoring the performance of carbon membranes for C_2H_4/C_2H_6 separation based on tuning the CMS pyrolysis conditions such as the final pyrolysis temperature, heating rates and the pyrolysis atmosphere has also been demonstrated.

Acknowledgments

The authors thank The Dow Chemical Co., for funding this work. The authors especially thank Mark Brayden and Marcos Martinez for helpful discussions and comments. The authors also acknowledge additional support provided by King Abdullah University of Science and Technology (KAUST).

Literature Cited

1. Gottschlich R. Energy Minimization of Separation Processes using Conventional/Membrane Hybrid Systems. Washington DC: US Dept. of Energy; 1990.
2. Robinson S, Jubin R, Choate B. Materials for Separation Technology: Energy and Emmision Reduction Opportunities. Washington DC: US Dept. of Energy; 2005.
3. Eldridge RB. Olefin paraffin separation technology: a review. *Ind Eng Chem Res.* 1993;32:2208–2212.
4. Caballero JA, Grossmann IE, Keyvani M, Lenz ES. Design of hybrid distillation-vapor membrane separation systems. *Ind Eng Chem Res.* 2009;48:9151–9162.
5. Rungta M, Xu L, Koros WJ. Carbon molecular sieve dense film membranes derived from Matrimid® for ethylene/ethane separation. *Carbon.* 2012;50:1488–1502.
6. Baker RW. Future directions of membrane gas separation technology. *Ind Eng Chem Res.* 2002;41:1393–1411.
7. Ozokwelu D. Hybrid Separations/Distillation Technology: Research Opportunities for Energy and Emissions Reduction. Washington DC: US Dept. of Energy; 2005.
8. Koros WJ. Evolving beyond the thermal age of separation processes: membranes can lead the way. *AIChE J.* 2004;50:2326–2334.
9. Chan SS, Wang R, Chung TS, Liu Y. C-2 and C-3 hydrocarbon separations in poly(1,5-naphthalene-2,2′-bis(3,4-phthalic) hexafluoropropane) diimide (6FDA-1,5-NDA) dense membranes. *J Membr Sci.* 2002;210:55–64.
10. Chan SS, Chung T-S, Liu Y, Wang R. Gas and hydrocarbon (C2 and C3) transport properties of co-polyimides synthesized from 6FDA and 1,5-NDA (naphthalene)/durene diamines. *J Membr Sci.* 2003;218:235–245.
11. Tanaka K, Taguchi A, Hao J, Kita H, Okamoto K. Permeation and separation properties of polyimide membranes to olefins and paraffins. *J Membr Sci.* 1996;121:197–207.
12. Staudt-Bickel C, Koros WJ. Olefin/paraffin gas separations with 6FDA-based polyimide membranes. *J Membr Sci.* 2000;170:205–214.

13. Koros WJ, Mahajan R. Pushing the limits on possibilities for large scale gas separation: which strategies? *J Membr Sci.* 2000;175:181–196.
14. Robeson LM. Correlation of separation factor versus permeability for polymeric membranes. *J Membr Sci.* 1991;62:165–185.
15. Robeson LM. The upper bound revisited. *J Membr Sci.* 2008;320: 390–400.
16. Freeman BD. Basis of permeability/selectivity tradeoff relations in polymeric gas separation membranes. *Macromolecules.* 1999;32:375–380.
17. Haraya K, Obata K, Itoh N, Shndo Y, Hakuta T, Yoshitome H. Gas permeation and separation by an asymmetric polyimide hollow fiber membrane. *J Membr Sci.* 1989;41:23–35.
18. Barrer RM. Activated diffusion in membranes. *T Faraday Soc.* 1939;35:0644–0655.
19. van Amerongen GJ. The permeability of different rubbers to gases and its relation to diffusivity and solubility. *J Appl Phys.* 1946;17:972–985.
20. Barrer RM, Skirrow G. Transport and equilibrium phenomena in gas elastomer systems. *1. Kinetic phenomena. J Polym Sci.* 1948;3:549–563.
21. van Krevelen DW. Properties of Polymers. 3rd ed. Amsterdam; The Netherlands: Elsevier Science; 1997.
22. Burns RL, Koros WJ. Defining the challenges for C3H6/C3H8 separation using polymeric membranes. *J Membr Sci.* 2003;211:299–309.
23. Semenova SI. Polymer membranes for hydrocarbon separation and removal. *J Membr Sci.* 2004;231:189–207.
24. Das M. Membranes for Olefin/Paraffin Separations [PhD thesis]. Atlanta, GA: Georgia Institute of Technology; 2009.
25. Chen CC. Thermally Crosslinked Polyimide Hollow Fiber Membranes for Natural Gas Purification [PhD thesis]. Atlanta, GA: Georgia Institute of Technology; 2011.
26. Pye DG, Hoehn HH, Panar M. Measurement of gas permeability of polymers. I. Permeabilities in constant volume/variable pressure apparatus. *J Appl Polym Sci.* 1976;20:1921–1931.
27. Pye DG, Hoehn HH, Panar M. Measurement of gas permeability of polymers. II. Apparatus for determination of permeabilities of mixed gases and vapors. *J Appl Polym. Sci.* 1976;20:287–301.
28. Ilinitch OM, Semin GL, Chertova MV, Zamaraev KI. Novel polymeric membranes for separation of hydrocarbons. *J Membr Sci.* 1992;66:1–8.
29. Ilinich OM, Zamaraev KI. Separation of ethylene and ethane over polyphenyleneoxides membranes: transient increase of selectivity. *J Membr Sci.* 1993;82:149–155.
30. Teplyakov V, Meares P. Correlationaspects of the selective gas permeabilities of polymeric materials and membranes. *Gas Sep Purif.* 1990;4:66–74.
31. Breck DW. Zeolite Molecular Sieves: Structure, Chemistry and Use. New York, NY: John Wiley & Sons, Inc.; 1974.
32. Petropolous JH. Mechanisms and theories for sorption and diffusion of gases in polymers. In: Paul DR, Yampol'skii YP. Polymeric Gas Separation Membranes. Boca Raton, FL: CRC Press; 1994:17–82.
33. Koros WJ, Paul DR, Huvard GS. Energetics of gas sorption in glassy polymers. *Polymer.* 1979;20:956–960.
34. Koros WJ, Paul DR. Design considerations for measurement of gas sorption in polymers by pressure decay. *J Polym Sci Pt B.* 1976;14: 1903–1907.
35. Costello LM, Koros WJ. Temperature-dependence of gas sorption and transport properties in polymers: measurement and applications. *Ind Eng Chem Res.* 1992;31:2708–2714.
36. Brandt WW. Model calculation of the temperature dependence of small molecule diffusion in high polymers. *J Phys Chem.* 1959;63: 1080–1084.
37. Merkel T, Blanc R, Zeid J, Suwarlim A, Firat B, Wijmans H, Asaro M, Greene M. Separation of Olefin/Paraffin Mixtures with Carrier Facilitated Membranes. Washington DC: US Dept. of Energy; 2007.
38. Faiz R, Li K. Olefin/paraffin separation using membrane based facilitated transport/chemical absorption techniques. *Chem Eng Sci.* 2012;73:261–284.
39. Ho WS, Dalrymple DC. Facilitated transport of olefins in Ag+-containing polymer membranes. *J Membr Sci.* 1994;91:13–25.
40. Ho WS, Doyle G, Savage DW, Pruett RL. Olefin separations via complexation with cuprous diketonate. *Ind Eng Chem Res.* 1988;27: 334–337.
41. Pinnau I, Toy LG. Solid polymer electrolyte composite membranes for olefin/paraffin separation. *J Membr Sci.* 2001;184:39–48.
42. Azhin M, Kaghazchi T, Rahmani M. A review on olefin/paraffin separation using reversible chemical complexation technology. *J Ind Eng Chem.* 2008;14:622–638.
43. Singh A, Koros WJ. Significance of entropic selectivity for advanced gas separation membranes. *Ind Eng Chem Res.* 1996;35:1231–1234.
44. Ruthven DM. Molecular sieve separations. *Chem Ing Tech.* 2011;83: 44–52.
45. Agarwal K, John M, Pai S, Newalkar BL, Bhargava R, Choudary NV. SAPO-34 assisted C3 separation: modeling and simulation. *Microporous Mesoporous Mater.* 2010;132:311–318.
46. Ruthven DM, Reyes SC. Adsorptive separation of light olefins from paraffins. *Microporous Mesoporous Mater.* 2007;104:59–66.
47. Karger J, Ruthven DM. Diffusion in Zeolites and other Microporous Solids. New York: John Wiley & Sons, Inc.; 1992.
48. Bloch ED, Queen WL, Krishna R, Zadrozny JM, Brown CM, Long JR. Hydrocarbon separations in a metal organic framework with open iron(II) coordination sites. *Science.* 2012;335:1606–1610.
49. Yang RT. Adsorbents: Fundamentals and Applications. Hoboken, NJ: John Wiley & Sons, Inc.; 2003.
50. Li K, Olson DH, Seidel J, Emge TJ, Gong H, Zeng H, Li J. Zeolitic imidazolate frameworks for kinetic separation of propane and propene. *J Am Chem Soc.* 2009;131:10368–10369.
51. Zhang C, Dai Y, Johnson JR, Karvan O, Koros WJ. High performance ZIF-8/6FDA-DAM mixed matrix membrane for propylene/propane separations. *J Membr Sci.* 2012;389:34–42.
52. Zhang C, Lively RP, Zhang K, Johnson JR, Karvan O, Koros WJ. Unexpected molecular sieving properties of zeolitic imidazolate framework-8. *J Phys Chem.* 2012;3:2130–2134.
53. Bae T-H, Lee JS, Qiu W, Koros WJ, Jones CW, Nair S. A high performance gas separation membrane containing submicrometer sized metal organic framework crystals. *Angew Chem Int Ed.* 2010;49: 9863–9866.
54. Dai Y, Johnson JR, Karvan O, Sholl DS, Koros WJ. Ultem®/ZIF-8 mixed matrix hollow fiber membranes for CO2/N2 separations. *J Membr Sci.* 2012;401-402:76–82.
55. Ordonez MJC, Balkus KJ, Ferraris JP, Musselman IH. Molecular sieving realized with ZIF-8/Matrimid mixed-matrix membranes. *J Membr Sci.* 2010;361:28–37.
56. Pan Y, Lai Z. Sharp separation of C2/C3 hydrocarbon mixtures by zeolitic imidazolate framework-8 (ZIF-8) membranes synthesized in aqueous solutions. *Chem Commun.* 2011;47:10275.
57. Gücüyener C, van den Bergh J, Gascon J, Kapteijn F. Ethane/ethene separation turned on its head: selective ethane adsorption on the metal organic framework ZIF-7 through a gate-opening mechanism. *J Am Chem Soc.* 2010;132:17704–17706.
58. Chmelik C, Freude D, Bux H, Haase J. Ethene/ethane mixture diffusion in the MOF sieve ZIF-8 studied by MAS PFG NMR diffusometry. *Microporous Mesoporous Mater.* 2011;147:135–141.
59. Bux H, Chmelik C, van Baten JM, Krishna R, Caro J. Novel MOF-membrane for molecular sieving predicted by IR-diffusion studies and molecular modeling. *Adv Mater.* 2010;22:4741–4743.
60. Bux H, Chmelik C, Krishna R, Caro J. Ethene/ethane separation by the MOF membrane ZIF-8: molecular correlation of permeation, adsorption, diffusion. *J Membr Sci.* 2011;369:284–289.
61. Chmelik C, Bux H, Voss H, Caro J. Adsorption and diffusion: basis for molecular understanding of permeation through molecular sieve membranes. *Chem Ing Tech.* 2011;83:104–112.
62. Moore TT, Mahajan R, Vu DQ, Koros WJ. Hybrid membrane materials comprising organic polymers with rigid dispersed phases. *AIChE J.* 2004;50:311–321.
63. Díaz K, López-González M, del Castillo LF, Riande E. Effect of zeolitic imidazolate frameworks on the gas transport performance of ZIF8-poly(1,4-phenylene ether-ether-sulfone) hybrid membranes. *J Membr Sci.* 2011;383:206–213.
64. Ploegmakers J, Japip S, Nijmeijer K. Mixed matrix membranes containing MOFs for ethylene/ethane separation Part A: membrane preparation and characterization. *J Membr Sci.* 2013;428:445–453.
65. Marsh H. Introduction to Carbon Science. London, UK: Butterworths; 1989.
66. Jenkins GM, Kawamura K. Polymeric Carbons: Carbon Fiber, Glass and Char. London, UK: Cambridge University Press; 1976.
67. Steel KM, Koros WJ. An investigation of the effects of pyrolysis parameters on gas separation properties of carbon materials. *Carbon.* 2005;43:1843–1856.
68. Kiyono M, Williams PJ, Koros WJ. Effect of pyrolysis atmosphere on separation performance of carbon molecular sieve membranes. *J Membr Sci.* 2010;359:2–10.

69. Singh-Ghosal A, Koros WJ. Air separation properties of flat sheet homogeneous pyrolytic carbon membranes. *J Membr Sci*. 2000;174: 177–188.
70. Steel KM. Carbon Membranes for Challenging Gas Separations [PhD thesis]. Austin, TX: The University of Texas; 2000.
71. Pierson HO. Handbook of Carbon, Graphite, Diamond, and Fullerenes. New York: Noyes Publication; 1993.
72. Vu DQ. Formation and Characterization of Asymmetric Carbon Molecular Sieve and Mixed Matrix Membranes for Natural Gas Purification [PhD thesis]. Austin, TX: The University of Texas; 2001.
73. Williams PJ. *Analysis of factors influencing the performance of CMS membranes for gas separation[PhD thesis]*. Atlanta, GA: Georgia Institute of Technology; 2006.
74. Xu L, Rungta M, Brayden MK, Martinez MV, Stears BA, Barbay GA, Koros WJ. Olefins-selective asymmetric carbon molecular sieve hollow fiber membranes for hybrid membrane-distillation processes for olefin/paraffin separations. *J Membr Sci*. 2012;423-424:314–323.
75. Fuertes AB, Menendez I. Separation of hydrocarbon gas mixtures using phenolic resin-based carbon membranes. *Sep Purif Technol*. 2002;28:29–41.
76. Centeno TA, Vilas JL, Fuertes AB. Effects of phenolic resin pyrolysis conditions on carbon membrane performance for gas separation. *J Membr Sci*. 2004;228:45–54.
77. Hayashi J, Mizuta H, Yamamoto M, Kusakabe K, Morooka S, Suh SH. Separation of ethane/ethylene and propane/propylene systems with a carbonized BPDA-pp'ODA polyimide membrane. *Ind Eng Chem Res*. 1996;35:4176–4181.
78. Okamoto K, Kawamura S, Yoshino M, Kita H. Olefin/paraffin separation through carbonized membranes derived from an asymmetric polyimide hollow fiber membrane. *Ind Eng Chem Res*. 1999;38: 4424–4432.
79. Suda H, Haraya K. Alkene/alkane permselectivities of a carbon molecular sieve membrane. *Chem Commun*. 1997:93–94.
80. Barsema JN, van der Vegt NFA, Koops GH, Wessling M. Carbon molecular sieve membranes prepared from porous fiber precursor. *J Membr Sci*. 2002;205:239–246.
81. Karvan O, Johnson JR, Williams PJ, Koros WJ. A pilot-scale system for carbon molecular sieve hollow fiber membrane manufacturing. *Chem Eng Technol*. 2013;36:53–61.
82. Xu L, Rungta M, Koros WJ. Matrimid® derived carbon molecular sieve hollow fiber membranes for ethylene/ethane separation. *J Membr Sci*. 2011;380:138–147.
83. Kiyono M, Williams PJ, Koros WJ. Effect of polymer precursors on carbon molecular sieve structure and separation performance properties. *Carbon*. 2010;48:4432–4441.
84. Grisdale RO. The properties of carbon contacts. *J Appl Phys*. 1953;24:1288–1296.
85. Singh R, Koros WJ. Carbon molecular sieve membrane performance tuning by dual temperature secondary oxygen doping (DTSOD). *J Membr Sci*. 2013;427:472–478.
86. Olson DH, Camblor MA, Villaescusa LA, Kuehl GH. Light hydrocarbon sorption properties of pure silica Si-CHA and ITQ-3 and high silica ZSM-58. *Microporous Mesoporous Mater*. 2004;67:27–33.
87. Dai W, Scheibe M, Li L, Guan N, Hunger M. Effect of the methanol-to-olefin conversion on the PFG NMR self-diffusivities of ethane and ethene in large-crystalline SAPO-34. *J Phys Chem C*. 2011; 116:2469–2476.
88. Romero-Perez A, Aguilar-Armenta G. Adsorption kinetics and equilibria of carbon dioxide, ethylene, and ethane on 4A(CECA) zeolite. *J Chem Eng*. 2010;55:3625–3630.
89. Centeno TA, Fuertes AB. Supported carbon molecular sieve membranes based on a phenolic resin. *J Membr Sci*. 1999;160:201–211.
90. Stoeckli HF. Microporous carbons and their characterization: the present state of the art. *Carbon*. 1990;28:1–6.
91. Reid C, Sherwood TK. The Properties of Gases and Liquids: Their Estimation and Correlation. New York: Mcgraw-Hill; 1976.
92. Hirschfelder, Oakland K. Molecular Theory of Gases and Liquids. New York, NY: Wiley Interscience; 1964.
93. Teramoto M, Matsuyama H, Yamashiro T, Katayama Y. Separation of ethylene from ethane by supported liquid membranes containing silver-nitrate as a carrier. *J Chem Eng*. 1986;19:419–424.
94. Eriksen OI, Aksnes E, Dahl IM. Facilitated transport of ethene through nafion membranes.1. Water swollen membranes. *J Membr Sci*. 1993;85:89–97.
95. Tsou DT, Blachman MW, Davis JC. Silver-facilitated olefin/paraffin separation in a liquid membrane contactor system. *Ind Eng Chem Res*. 1994;33:3209–3216.
96. Bessarabov DG, Sanderson RD, Jacobs EP, Beckman IN. High-efficiency separation of an ethylene ethane mixture by a large-scale liquid-membrane contactor containing flat-sheet nonporous polymeric gas-separation membranes and a selective flowing-liquid absorbent. *Ind Eng Chem Res*. 1995;34:1769–1778.
97. Teramoto M, Matsuyama H, Yamashiro T, Okamoto S. Separation of ethylene from ethane by a flowing liquid membrane using silver-nitrate as a carrier. *J Membr Sci*. 1989;45:115–136.
98. Nymeijer K, Visser T, Assen R, Wessling M. Super selective membranes in gas-liquid membrane contactors for olefin/paraffin separation. *J Membr Sci*. 2004;232:107–114.
99. Ryu JH, Lee H, Kim YJ, Kang YS, Kim HS. Facilitated olefin transport by reversible olefin coordination to silver ions in a dry cellulose acetate membrane. *Chem Eur J*. 2001;7:1525–1529.
100. Kim HS, Ryu JH, Kim H, Ahn BS, Kang YS. Reversible olefin complexation by silver ions in dry poly(vinyl methyl ketone) membrane and its application to olefin/paraffin separations. *Chem Commun*. 2000:1261–1262.

Manuscript received Nov. 1, 2012, and revision received Mar. 10, 2013.